

The JCMT Gould Belt Survey: SCUBA-2 observations of radiative feedback in NGC1333

J. Hatchell^{1*}, T. Wilson¹, E. Drabek¹, E. Curtis², J. Richer^{2,3}, D. Nutter⁴,
J. Di Francesco^{5,6} and D. Ward-Thompson⁷ on behalf of the JCMT GBS consortium⁸.

¹*Physics and Astronomy, University of Exeter, Stocker Road, Exeter EX4 4QL*

²*Astrophysics Group, Cavendish Laboratory, Madingley Road, Cambridge CB3 0HE*

³*Kavli Institute for Cosmology, Cambridge, Madingley Road, Cambridge, CB3 0HA*

⁴*Department of Physics and Astronomy, Cardiff University, Queen's Buildings, The Parade, Cardiff CF24 3AA*

⁵*National Research Council of Canada Radio Astronomy Program, 5071 West Saanich Rd., Victoria, BC, V9E 2E7, Canada*

⁶*University of Victoria, Department of Physics and Astronomy, PO Box 3055, STN CSC, Victoria, BC, V8W 3P6, Canada*

⁷*Jeremiah Horrocks Institute, University of Central Lancashire, Preston, Lancashire, PR1 2HE*

⁸*A complete list of survey members is given in Appendix A (online only).*

Sept12

ABSTRACT

We present observations of NGC1333 from SCUBA-2 on JCMT, observed as a JCMT Gould Belt Survey pilot project during the shared risk campaign when the first of four arrays was installed at each of 450 and 850 microns. Temperature maps are derived from 450 μ m and 850 μ m ratios under the assumption of constant dust opacity spectral index $\beta = 1.8$. Temperatures indicate that the dust in the northern (IRAS 6/8) region of NGC1333 is hot, 20–40 K, due to heating by the B star SVS3, other young stars in the IR/optically visible cluster, and embedded protostars. Other luminous protostars are also identified by temperature rises at the 17'' resolution of the ratio maps (0.02 pc assuming a distance of 250 pc for Perseus). The extensive heating raises the possibility that the radiative feedback may lead to increased masses for the next generation of stars.

Key words: ISM – dust, extinction: stars – formation: submillimeter

1 INTRODUCTION

Gas temperature plays a role in controlling star formation in dense cores through thermal support (Jeans 1902). The thermal Jeans length may ultimately control the sub-fragmentation of cloud cores once turbulent motions have decayed and cores become coherent (Goodman et al. 1998; Myers 1983). Heating of protostellar cores suppresses sub-fragmentation (Bate 2009; Offner et al. 2009; Urban, Martel & Evans 2010; Chabrier & Hennebelle 2011) and is potentially an important factor in the formation of massive stars (along with magnetic fields, competitive accretion, and other factors; see Hennebelle & Commercon 2012 for a review).

Observationally, several techniques exist for measuring temperatures of molecular gas, including CO excitation temperatures (e.g. Curtis, Richer & Buckle 2010; Ladd, Myers & Goodman 1994) and the ammonia ladder (e.g. Huttemeister et al. 1993). The dust colour temperature T_d provides an alternative estimate of the gas temperature: at high molecular hydrogen densities $n_{H_2} > 10^{4.5} \text{ cm}^{-2}$, where gas-grain collisions dominate the gas heating, the dust and gas temperatures are well coupled (Goldsmith 2001).

Dust colour temperatures rely on fitting dust continuum fluxes to an opacity-modified blackbody spectrum, a method which is being applied very successfully to make temperature and column density maps of nearby star-forming regions from Herschel data based on fits from 160 μ m to 500 μ m (André et al. 2010).

In this paper we apply dust temperature methods to 450 μ m and 850 μ m submillimetre (submm) data from SCUBA-2 on the James Clerk Maxwell Telescope (JCMT; Holland et al. 2006), using a similar technique to that developed for SCUBA (Kramer et al. 2003). There are benefits in using long-wavelength mm/submm data for dust temperatures (as long as the data points are not entirely on the Rayleigh-Jeans tail). When temperature varies along the line-of-sight, dust continuum fluxes are emission-averaged and hence weighted towards the hottest dust. Small fractions of hot dust can dominate the mid-infrared (mid-IR) even though they contain only a small fraction of the total dust mass, as is evident from protostellar spectral energy distributions (e.g. Enoch et al. 2009). For sources with a simple geometry, this temperature variation issue can be circumvented by radiative transfer modelling, but this is not a realistic option for complex star-forming regions. Also, in high column density regions, the dust emission at mid-IR wavelengths can become optically thick, weighting the results towards the front

* E-mail: hatchell@astro.ex.ac.uk

side of the cloud and low-opacity photon escape routes. The $14''$ beam full width half maximum (FWHM) of JCMT at $850\ \mu\text{m}$ provides an improvement in angular resolution over Herschel at $500\ \mu\text{m}$ ($37''$ FWHM), which is advantageous in dense clusters and when determining the relative location of heating sources and cores.

Here we apply the dust colour temperature method to the young cluster NGC1333 in Perseus. NGC1333 is a young cluster well studied in the mm/submm (Sandell & Knee 2001; Hatchell et al. 2007; Kirk, Johnstone & Tafalla 2007; Enoch et al. 2006; Curtis, Richer & Buckle 2010; Curtis et al. 2010); for general background see Walawender et al. (2008).

2 METHOD

2.1 Observations and data reduction

NGC1333 was observed on February 21–22 2010 and March 4th and 7th 2010 as a JCMT Gould Belt Survey (Ward-Thompson et al. 2007) pilot project in the SCUBA-2 shared risk (S2SRO) campaign, during which only one array out of the final four was available at each of $850\ \mu\text{m}$ and $450\ \mu\text{m}$ (Holland et al. 2006). These observations were among the first made with SCUBA-2. The weather conditions were good, JCMT Band 2 with 225 GHz opacity $\tau_{225} = 0.05\text{--}0.07$. Two overlapping $15'$ diameter circular regions ('PONG900' mapping mode; Jenness et al. 2011) were targeted, with map centres offset $10'$ to the north and south from RA(2000) = $03^{\text{h}}\ 29^{\text{m}}\ 00^{\text{s}}$, Dec. (2000) = $31^{\circ}\ 18'\ 00''$. These fully-sampled $15'$ -diameter regions were surrounded by $4'$ borders that were scanned at lower sensitivity by decreasing numbers of the array pixels.

Molecular lines contribute to the signal in the SCUBA-2 $850\ \mu\text{m}$ continuum bandwidth, with the most significant contamination at 345 GHz due to the CO $J = 3\text{--}2$ line (Drabek et al. 2012). The CO contamination was removed during the $850\ \mu\text{m}$ reduction using the HARP $^{12}\text{CO}\ 3\text{--}2$ integrated intensity map (Curtis, Richer & Buckle 2010) converted to a CO contamination map using a contamination factor of $0.66\ \text{mJy/beam}/(\text{K km s}^{-1})$ appropriate to Band 2 weather with an average $\tau_{225} = 0.06$ (Drabek et al. 2012). The $850\ \mu\text{m}$ map was re-reduced in June 2012 using the development version of the data reduction package SMURF (Jenness et al. 2011, version of 2nd May 2012) with astronomical signal (AST) masking based on earlier versions of the reductions and gridding to $6''$ pixels. The CO contamination map was injected during the $850\ \mu\text{m}$ reduction process as a fake source with a negative multiplying factor of $-1/\text{FCF}$ where FCF is the flux conversion factor (see below). In this way, the CO emission was subtracted from the timeseries fluxes during the reduction, matching the spatial filtering inherent in SCUBA-2 map reconstruction and resulting in an $850\ \mu\text{m}$ map which is corrected for CO line contamination. The $450\ \mu\text{m}$ map was re-reduced in May 2012 using the same SMURF version, with AST masking, without CO contamination removal, and gridded to $4''$ pixels. Both the $850\ \mu\text{m}$ and $450\ \mu\text{m}$ maps are insensitive to emission on scales greater than the on-sky footprint of the array ($4'$ for the single-array S2SRO) due to common-mode subtraction of atmospheric emission across the array.

Maps were calibrated by multiplying by flux conversion factors (FCFs) of $653 \pm 49\ \text{Jy/beam/picoWatt}$ and $511 \pm 31\ \text{Jy/beam/pW}$ at $850\ \mu\text{m}$ and $450\ \mu\text{m}$ respectively, derived from the six observations of the submm calibrator CRL618 (Dempsey et al. 2012). The average beam FWHM were measured to be

$14.4'' \pm 0.15''$ ($850\ \mu\text{m}$) and $9.8'' \pm 0.23''$ ($450\ \mu\text{m}$) consistent with the observatory standards of $14.2''/9.4''$.

Of the 18 maps observed, 12 were selected for mosaicking, six each for the north and south centres, with six rejected due to telescope tracking errors. The resulting mosaics have pixel-to-pixel 1σ noise levels of 7.8 and 130 mJy per $14.4''/9.8''$ beam on $6''/4''$ pixels at $850\ \mu\text{m}/450\ \mu\text{m}$ respectively (an average over the north and south regions, which have noise levels +4% higher and lower respectively), roughly a factor two deeper than SCUBA (Sandell & Knee 2001; Hatchell et al. 2005). Calculating the equivalent point-source sensitivity at a resolution equal to the beam area, these observations meet the JCMT Gould Belt Survey 3 mJy target at $850\ \mu\text{m}$ while achieving 50 mJy point source sensitivity at $450\ \mu\text{m}$. The central, overlap region of the map has a still lower noise level by roughly $\sqrt{2}$. The pixel-to-pixel noise estimates do not completely represent the noise levels in larger-scale fluctuations which were measured from histograms of the pixel values to be 14 mJy/beam and 150 mJy/beam respectively.

2.2 Ratio and temperature maps

For optically thin emission, the flux ratio between the two wavelengths $450\ \mu\text{m}$ and $850\ \mu\text{m}$ depends solely on the dust opacity and temperature. The dust opacity is standardly parameterised at long wavelengths as a power law $\kappa \propto \nu^\beta$ (Hildebrand 1983). The 450/850 flux ratio is then

$$\frac{S_{450}}{S_{850}} = \left(\frac{850}{450}\right)^{3+\beta} \left(\frac{\exp(hc/\lambda_{850}kT_d) - 1}{\exp(hc/\lambda_{450}kT_d) - 1}\right) \quad (1)$$

where T_d is the dust temperature and λ_{850} and λ_{450} are $850\ \mu\text{m}$ and $450\ \mu\text{m}$ wavelengths respectively.

Higher 450/850 flux ratios can be produced either by higher dust temperatures, a higher opacity index β , or both. Separating the two requires data at additional wavelengths, e.g. a joint analysis with the Herschel $250\ \mu\text{m}$ and $500\ \mu\text{m}$ datasets, which is planned for future work beyond the scope of this Letter. Higher dust temperatures are caused by heating, whereas grain growth can change β by raising the typical sizes and absorption wavelengths of grains. β typically lies in the range 1 to 2, depending on the type and clumpiness of grains. Increases in β have been observed in protoplanetary disks (e.g. Ubach et al. 2012) and low-density clouds (Martin et al. 2012) but to date there is little knowledge of changes in pre/protostellar cores, a situation that should improve rapidly with availability of SCUBA-2 and Herschel data. There is a suggestion that icy mantles increase towards the inner parts of the Class 0 source B335 though not enough to significantly affect β (Doty et al. 2010).

The flux ratio map was created from the $450\ \mu\text{m}$ and CO-subtracted $850\ \mu\text{m}$ maps, which were scaled to Jy/pixel with any negative fluxes removed. The $450\ \mu\text{m}$ map was convolved with a 2-dimensional Gaussian representing the $850\ \mu\text{m}$ $14.4''$ primary beam, and the $850\ \mu\text{m}$ map similarly convolved with a $450\ \mu\text{m}$ $9.8''$ primary beam to match angular resolution. The cross-convolution procedure produced more consistent matched beams than simply convolving the $450\ \mu\text{m}$ map to the $850\ \mu\text{m}$ resolution and was needed for the S2SRO data to avoid artefacts in the ratio map. The flux ratio map was created by dividing the resolution-matched, re-gridded $450\ \mu\text{m}$ and $850\ \mu\text{m}$ maps with values in each map below 5σ blanked. For a fixed value of the dust opacity β , Equation 1 was used to convert the ratio map into a temperature map, with an additional cut of temperatures with variance $> 30\ \text{K}$ applied. The

effective angular resolution of the ratio and temperature maps is $17.4''$. The systematic uncertainty in the ratio maps due to calibration at each wavelength is 15%. The large-scale filtering inherent in S2SRO maps adds edge effects and systematic offsets to the ratios which will be quantified by future modelling. These effects are smallest where bright compact structures dominate the fluxes, as is the case for most of NGC1333.

3 RESULTS

The S2SRO 850 μm map of NGC1333 is presented in Fig. 1(a) as a finding chart. SCUBA cores are labelled with their HRF2005 numbering (Hatchell et al. 2005, 2007, hereafter HRF nn) and protostars identified from *Spitzer* mid-IR detections are marked (Gutermuth et al. 2008; Jørgensen et al. 2006). Further identifications of sources in NGC1333 can be found in Sandell & Knee (2001). Figure 1(b) shows the 450 μm map of this region. The 450 μm dataset from S2SRO is sensitive and stable enough for the filamentary structure to be seen clearly, as it is not dominated by the large-scale noise artefacts which limited analysis of the SCUBA 450 μm data (Sandell & Knee 2001; Hatchell et al. 2005).

In Fig. 1(c) we plot the dust temperature in NGC1333 assuming a constant dust opacity spectral index of $\beta = 1.8$. This choice of β is consistent with the popular OH5 dust model ($\beta = 1.85$; Ossenkopf & Henning 1994), with recent results for dense cores from Planck and Herschel (Juvella et al. 2011; Stutz et al. 2010), and with comparisons of SCUBA and near-infrared opacities (Shirley et al. 2011). Although variation in the 450/850 ratio may also be due to variation in β (to be investigated in future work), as NGC1333 contains several luminous protostars and a reflection nebula, it is reasonable as a first approximation to assume that the variation is dominated by temperature. A higher value for β would result in lower temperatures for the same ratios: temperatures of 10 K, 20 K and 40 K at $\beta = 1.8$ fall to 8.5 K, 14 K and 20 K at $\beta = 2.2$.

Filaments and ambient cloud material generally show dust temperatures of 10 K (corresponding to 450/850 ratios of around 4;). These temperatures are typical of the cold dense interstellar medium (Evans et al. 2001; Shirley, Evans & Rawlings 2002). Towards the protostars, beam-averaged temperatures rise to 12–15 K, consistent with SCUBA-based models of low-mass Class 0 and 1 protostars (Shirley, Evans & Rawlings 2002; Young et al. 2003) and with the Herschel analysis of CB244 (Stutz et al. 2010). Some of the more luminous protostars show notably higher dust temperatures as discussed below. The temperature does not, however, rise towards all protostars identified by *Spitzer* mid-IR detections or outflows (Jørgensen et al. 2006; Hatchell et al. 2007; Gutermuth et al. 2008; Hatchell, Fuller & Richer 2007; Hatchell & Dunham 2009). Low-luminosity protostars have similar temperatures of 10–15 K to starless cores. The falling 450/850 ratios towards the map edge are almost certainly an artefact of the filtering of the large-scale background in the S2SRO map reconstruction, and not a physical effect due to falling β or temperature. Edge reconstruction should improve with data from the full SCUBA-2 array, which is sensitive to spatial scales a factor of two larger.

The most obvious feature in the temperature map is the warm northern region containing cores HRF45, 47, 54, 56, and 66 that shows widespread dust temperatures above 20 K. This region lies to the south of the optical cluster, and its dust is presumably heated by the stars in the optical cluster as well as the embedded protostellar population. The optically revealed cluster stars are dominated by the B5 star SVS3 (Strom, Vrba & Strom 1976; Straizys et al. 2002)

which lies on the edge of the dust to the northeast of HRF54, as marked in Fig. 1(a). SVS3 is a $138 L_{\odot}$ binary with an F2 companion (Connelley, Reipurth & Tokunaga 2008); the optically-visible NGC1333 reflection nebula and associated infrared source (IRAS 8; Jennings et al. 1987) is evidence its proximity to the dust cloud. The other main heating sources are embedded protostars. Core HRF45 is heated by SSTc2d J032901.6+312021 (Evans et al. 2009) as supported by its high temperature and identification as IRAS 6 (Jennings et al. 1987). Protostar SSTc2d J032907.8+312157 in HRF56 is also classified as a $27L_{\odot}$ luminosity source (Gutermuth et al. 2008; Evans et al. 2009). This luminosity is likely to be partially due to accretion and partially reprocessed flux from SVS3. The dust at this position is warm (~ 20 K), though not as warm as neighbouring HRF54 heated by SVS3 to form IRAS 8. The ridge containing HRF66 has elevated temperatures; a protostar embedded in HRF66 could explain some of this heating but a second source would also be necessary to heat the ridge to the southwest. Sources HRF47 and 53 are also warm (~ 20 K) but do not show temperature peaks. Core HRF47 contains a *Spitzer*-identified protostar, J032859.56+312146.7 (Jørgensen et al. 2006; Evans et al. 2009), but the closest *Spitzer* detection to HRF53 is SSTc2d J032905.18+312036.9 to the southeast where the dust temperature rises (Gutermuth et al. 2008; Evans et al. 2009).

An insight into the location of the heating sources can be made by comparison with ^{12}CO excitation temperatures $T_{\text{ex}}(\text{CO})$ (Curtis, Richer & Buckle 2010, Fig. 13). The ^{12}CO traces warm gas on the front side of the cloud (as the ^{12}CO is generally optically thick) but the submm dust emission is optically thin and traces heating through the cloud. Towards SVS3, the ^{12}CO temperature peaks sharply at over 40 K indicating heating of the front of the cloud. The dust temperature rise is more extensive, suggesting additional heating from embedded sources or sources behind the cloud, including SSTc2d J032905.18+312036.9. Towards the HRF45 and 47 cores, the dust and ^{12}CO excitation temperatures are similar (~ 40 –45 K), indicating that the heating sources lie near the front side of the cloud.

Further to the north, another B star, BD +30 549 or NGC1333 IRAS 9 classified as B8 (Jennings et al. 1987), lies close to HRF57 and 67 in projection which may explain raised dust temperatures of 15–17 K in these northern filaments. A significantly higher CO temperature, $T_{\text{ex}}(\text{CO})$ over 40 K, suggests that BD +30 549 lies in front of the cloud. Several protostars in other parts of the cloud are identifiable by their raised 450/850 ratios and temperatures. NGC 1333 IRAS 7 (HRF46) shows raised $T_{\text{ex}}(\text{CO}) \sim 35$ K and raised $T_{\text{dust}} \sim 20$ K to the northeast of the dense core. This could be due to the embedded source lying towards the front side of the cloud, or more likely in this case, hot CO lining a protostellar outflow cavity opening to the northeast (Curtis et al. 2010).

Deeply embedded sources or sources behind the cloud show the opposite effect with $T_{\text{d}} > T_{\text{ex}}(\text{CO})$. These include the SVS13 ridge (HRF43) and NGC 1333 IRAS 2 (HRF44). The HRF49 condensation shows a particularly strong dust temperature gradient from 10K in the southwest to over 40K at the northeast head of the condensation, heated by infrared source SSTc2d J032837.1+311331 (Gutermuth et al. 2008; Enoch et al. 2009). ^{12}CO excitation temperature maps (Curtis, Richer & Buckle 2010, Fig. 13) show no evidence for raised gas temperatures in this region indicating that the front of the core from which the optically-thick ^{12}CO escapes is cold and the star and the hot dust lie behind the dense core.

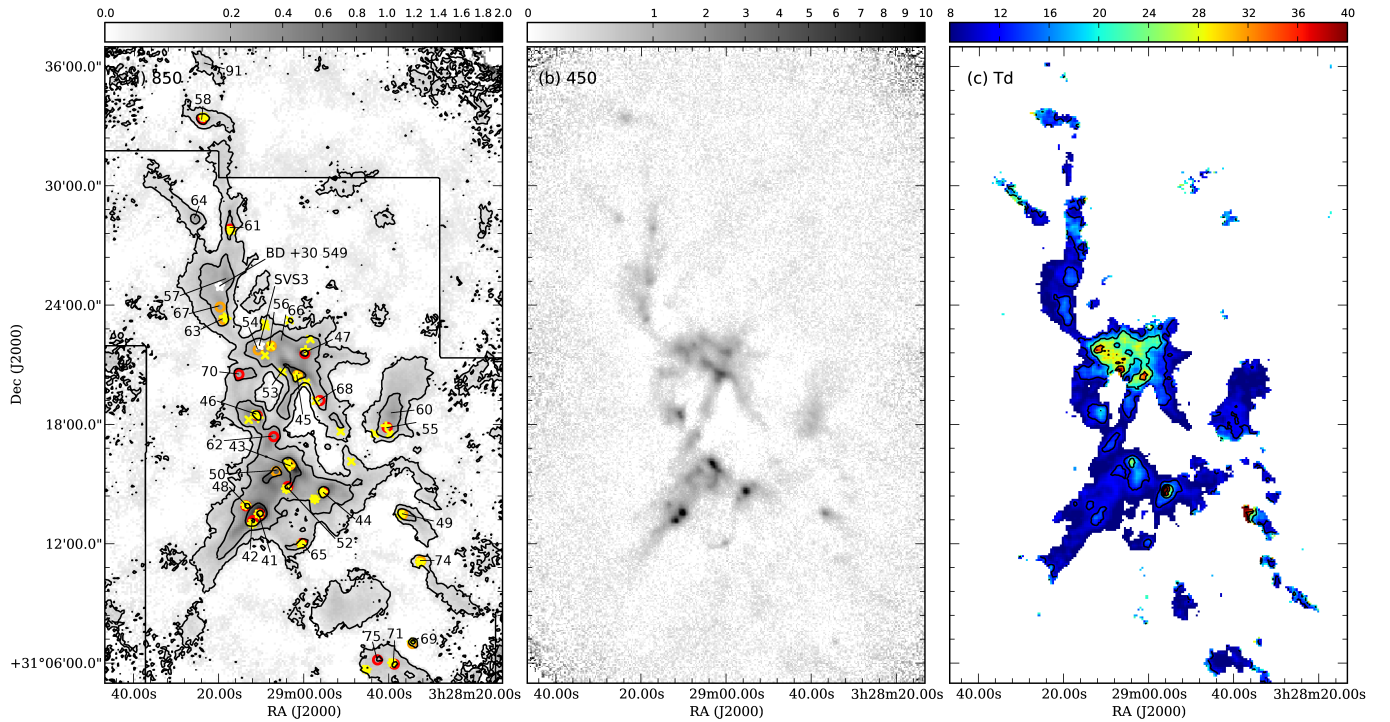


Figure 1. Left to right: (a) CO-subtracted S2SRO 850 μm map of NGC1333. Contours are at 0.02, 0.1, 0.5, 2.5 Jy/beam. The black line marks the CO subtraction region. Labels identify SCUBA sources (Hatchell et al. 2005) and the two B stars. Markers identify embedded protostars from Hatchell et al. (2007) (red circles for Class 0, orange circles for Class I), Jørgensen et al. (2006) (yellow +) and Gutermuth et al. (2008) (yellow \times). (b) S2SRO 450 μm map in Jy/beam. (c) Dust temperature T_d map at $\beta = 1.8$ in units of Kelvin. Contours are at $T_d = 12, 20,$ and 30 K.

4 DISCUSSION

Our observations show that star formation has raised 450/850 ratios in NGC1333. The absolute values of temperature in Fig. 1 depend on our assumption of $\beta = 1.8$, and increases in β may account for some of the 450/850 ratio rises towards dense cores. However, an explanation based on opacity alone would require extreme values of $\beta \sim 3$ towards the reflection nebula and luminous SVS13, whereas dust heating provides a simple explanation for ratio rises in these regions.

According to theory, heating increases thermal pressure which acts to stabilise cloud material against further fragmentation (Jeans 1902). The thermal Jeans length and Jeans mass scale as \sqrt{T} and $T^{3/2}$ respectively. Cores may be heated internally, potentially suppressing fragmentation resulting in more massive stars, or externally by earlier generations of stars, as recently investigated in G8.68–0.37 (Longmore et al. 2011). In NGC1333, there is no evidence that the northern region has fragmented with larger core separations than the rest of the region to date, presumably because the $1' - 1.5'$ core separation scales have been set by turbulent, rather than thermal, support (e.g. Chabrier & Hennebelle 2011). The local temperature rise in NGC1333 N due to the existing optical cluster and embedded protostars may, however, now inhibit the formation through fragmentation of further gravitational cores within the northern region. At the average molecular hydrogen density of NGC1333 N, $n_{\text{H}_2} \simeq 4 \times 10^4 \text{ cm}^{-3}$, the Jeans mass increases from 0.5 to 4 M_\odot as temperature rises from 10 to 40 K. If no further cores form, the existing protostars will accrete the remaining gravitationally bound gas (minus a fraction removed by outflows). The existing cores will produce more massive stars than they would have done in the absence of external heating. Hence the radiative

feedback from the existing cluster may influence the development of the next generation of stars.

There is possible evidence in the data here of the effect of external heating in promoting massive star formation in core HRF56. The embedded protostar SSTc2d J032907.8+312157 lies only 0.05 pc in projection from the B5 star SVS3 and on the edge of the optical nebula. If its current luminosity of $27L_\odot$ (Evans et al. 2009) is internally generated (rather than reprocessed emission from SVS3), and with a few M_\odot envelope still to accrete, HRF56 could be forming a second B star. Its lack of fragmentation could be influenced by heating from nearby SVS3. The nearby HRF54 core may be affected similarly in the future. We agree with Longmore et al. (2011) that this is a somewhat unsatisfactory circular argument as it requires a pre-existing massive star (SVS3) to provide the feedback, rather than a cluster of low-mass stars. Further to the south, HRF45/IRAS 6 has a current luminosity of $15L_\odot$ and a few M_\odot envelope so could also reach B-star status. This source, however, does not lie close to any such luminous star and a double radio detection indicates that it has already fragmented (Rodríguez, Anglada & Curiel 1999). Any further stars formed are likely to be typical AFGK-type cluster members since the remaining cores are low mass, at most a few M_\odot each. (Note that the total mass in NGC1333 N is only $\sim 20M_\odot$, assuming an average dust temperature of 20 K. Previous core mass calculations assumed fixed temperatures (Hatchell et al. 2007; Kirk, Johnstone & Tafalla 2007; Sandell & Knee 2001) or temperatures from IRAS (Sandell & Knee 2001). A future step will be to recalculate the masses of the NGC1333 N cores based on the dust temperatures and fluxes from the full SCUBA-2 Gould Belt survey data, which will have better spatial response and stabler calibration than the S2SRO data presented here).

Finally, in HRF54/IRAS8, radiative feedback by SVS3 may be promoting formation of an early B-type star with potentially devastating consequences for NGC1333 through widespread dissociation of the molecular gas and a halt to further star formation activity in the region. Possibly, the high-mass stars currently missing from the IMF of Perseus and other young low-mass star-forming regions (Evans et al. 2009) only form once radiative feedback from the existing clusters reaches a sufficiently high level. A further consequence is that massive stars are likely to form relatively late in molecular clouds, in the centre of clusters where the gas heating is greatest.

5 CONCLUSIONS

SCUBA-2 S2SRO observations show significantly raised dust temperatures around several luminous protostars in NGC1333, including SVS13 and IRAS 2. Assuming a dust opacity spectral index $\beta = 1.8$, the region on the southern edge of the optical reflection nebula is extensively heated to temperatures > 20 K, reaching 40 K close to the B star SVS3 and the embedded protostar IRS 6. A significant fraction of the energy input is from the optical cluster, and specifically the B star SVS3 illuminating the reflection nebula. Heating by the existing cluster is potentially biasing the star formation in the north of NGC1333 in favour of more massive stars.

NGC1333 will be observed again with the fully-commissioned SCUBA-2 as part of the JCMT Gould Belt Survey.

ACKNOWLEDGEMENTS

JH would like to thank all the staff at JAC, UKATC, and elsewhere who have worked so hard to make SCUBA-2 a reality, the JCMT Gould Belt Survey members (see Appendix A) for planning the SCUBA-2 survey, and Samantha Walker-Smith for help with protostellar core identifications.

REFERENCES

- André P. et al., 2010, *A&A*, 518, L102
 Bate M. R., 2009, *MNRAS*, 392, 1363
 Chabrier G., Hennebelle P., 2011, *A&A*, 534, A106
 Connelley M. S., Reipurth B., Tokunaga A. T., 2008, *AJ*, 135, 2496
 Curtis E. I., Richer J. S., Buckle J. V., 2010, *MNRAS*, 401, 455
 Curtis E. I., Richer J. S., Swift J. J., Williams J. P., 2010, *MNRAS*, 408, 1516
 Dempsey J. T. et al., 2012, *SPIE* in press; arXiv1208.4622
 Doty S. D., Tidman R., Shirley Y., Jackson A., 2010, *MNRAS*, 406, 1190
 Drabek E. et al., 2012, *MNRAS*, 426, 23
 Enoch M. L., Evans, II N. J., Sargent A. I., Glenn J., 2009, *ApJ*, 692, 973
 Enoch M. L. et al., 2006, *ApJ*, 638, 293
 Evans N. J. et al., 2009, *ApJS*, 181, 321
 Evans, II N. J., Rawlings J. M. C., Shirley Y. L., Mundy L. G., 2001, *ApJ*, 557, 193
 Goldsmith P. F., 2001, *ApJ*, 557, 736
 Goodman A. A., Barranco J. A., Wilner D. J., Heyer M. H., 1998, *ApJ*, 504, 223
 Gutermuth R. A. et al., 2008, *ApJ*, 674, 336
 Hatchell J., Dunham M. M., 2009, *A&A*, 502, 139
 Hatchell J., Fuller G. A., Richer J. S., 2007, *A&A*, 472, 187
 Hatchell J., Fuller G. A., Richer J. S., Harries T. J., Ladd E. F., 2007, *A&A*, 468, 1009
 Hatchell J., Richer J. S., Fuller G. A., Quattrough C. J., Ladd E. F., Chandler C. J., 2005, *A&A*, 440, 151
 Hennebelle P., Commerçon B., 2012, to appear in ‘The Labyrinth of Star Formation’, D. Stamatellos, S. Goodwin, and D. Ward-Thompson, eds., Springer, arXiv:1209.1786
 Hildebrand R. H., 1983, *QJRAS*, 24, 267
 Holland W. et al., 2006, in *Proceedings of the SPIE*, Vol. 6275, Society of Photo-Optical Instrumentation Engineers
 Huttemeister S., Wilson T. L., Henkel C., Mauersberger R., 1993, *A&A*, 276, 445
 Jeans J. H., 1902, *Royal Society of London Philosophical Transactions Series A*, 199, 1
 Jenness T., Berry D., Chapin E., Economou F., Gibb A., Scott D., 2011, in *ASP Conference Series*, Vol. 442, *Astronomical Data Analysis Software and Systems XX*, Evans I. N., Accomazzi A., Mink D. J., Rots A. H., eds., p. 281
 Jennings R. E., Cameron D. H. M., Cudlip W., Hirst C. J., 1987, *MNRAS*, 226, 461
 Jørgensen J. K. et al., 2006, *ApJ*, 645, 1246
 Juvela M. et al., 2011, *A&A*, 527, A111
 Kirk H., Johnstone D., Tafalla M., 2007, *ApJ*, 668, 1042
 Kramer C., Richer J., Mookerjee B., Alves J., Lada C., 2003, *A&A*, 399, 1073
 Ladd E. F., Myers P. C., Goodman A. A., 1994, *ApJ*, 433, 117
 Longmore S. N., Pillai T., Keto E., Zhang Q., Qiu K., 2011, *ApJ*, 726, 97
 Martin P. G., Roy A., Bontemps S., Miville-Deschênes M.-A., Ade P. A. R., 2012, *ApJ*, 751, 28
 Myers P. C., 1983, *ApJ*, 270, 105
 Offner S. S. R., Klein R. I., McKee C. F., Krumholz M. R., 2009, *ApJ*, 703, 131
 Ossenkopf V., Henning T., 1994, *A&A*, 291, 943
 Rodríguez L. F., Anglada G., Curiel S., 1999, *ApJS*, 125, 427
 Sandell G., Knee L. B. G., 2001, *ApJ*, 546, L49
 Shirley Y. L., Evans, II N. J., Rawlings J. M. C., 2002, *ApJ*, 575, 337
 Shirley Y. L., Huard T. L., Pontoppidan K. M., Wilner D. J., Stutz A. M., Bieging J. H., Evans, II N. J., 2011, *ApJ*, 728, 143
 Straizys V., Corbally C. J., Kazlauskas A., Černis K., 2002, *Baltic Astronomy*, 11, 261
 Strom S. E., Vrba F. J., Strom K. M., 1976, *AJ*, 81, 314
 Stutz A. et al., 2010, *A&A*, 518, L87
 Ubach C., Maddison S. T., Wright C. M., Wilner D. J., Lommen D. J. P., Koribalski B., 2012, *ArXiv e-prints*
 Urban A., Martel H., Evans, II N. J., 2010, *ApJ*, 710, 1343
 Walawender J., Bally J., Francesco J. D., Jørgensen J., Getman K., 2008, in ‘Handbook of Star Forming Regions, Volume I: The Northern Sky’, *ASP Monograph Publications*, Vol. 4., Reipurth, B., ed., p.308, p. 346
 Ward-Thompson D. et al., 2007, *PASP*, 119, 855
 Young C. H., Shirley Y. L., Evans, II N. J., Rawlings J. M. C., 2003, *ApJS*, 145, 111

**APPENDIX A: THE JCMT GOULD BELT SURVEY
CONSORTIUM**

The full members of the JCMT Gould Belt Survey consortium are P. Bastien, D. Berry, C. Brunt, J. Buckle, H. Butner, A. Cabral, P. Caselli, S. Chitsazzadeh, H. Christie, A. Chrysostomou, S. Coudé,, R. Curran, M. Currie, E. Curtis, C.J. Davis, W. Dent, E. Drabek, J. Di Francesco, M. Fich, J. Fiege, L. Fissel, P. Friberg, R. Friesen, G. Fuller, S. Graves, J. Greaves, J. Hatchell, M. Hogerheijde, W. Holland, T. Jenness, D. Johnstone, G. Joncas, J.M. Kirk, H. Kirk, L.B.G. Knee, B.C. Matthews, H. Matthews, J.C. Mottram, D. Nutter, J. Patience, J.E. Pineda, C. Quinn, J. Rawlings, R. Redman, M. Reid, J. Richer, E. Rosolowsky, S. Sadavoy, C. Salji, G. Schieven, N. Tohill, H. Thomas, S. Viti, S. Walker-Smith, D. Ward-Thompson, G.J. White, J. Wouterloot, J. Yates, and M. Zhu.